Comparison of cm- and mm-Wave Channel Characteristics between Autonomous Mobile Robots in a small I4.0 Manufacturing Facility

Sørensen, Troels Bundgaard; Bruun, Rasmus; Marcker, Rene Dam; E. Mogensen, Preben

Published in:
2022 25th International Symposium on Wireless Personal Multimedia Communications (WPMC)

DOI (link to publication from Publisher):
10.1109/WPMC55625.2022.10014913

Publication date:
2023

Document Version
Accepted author manuscript, peer reviewed version

Comparison of cm- and mm-Wave Channel Characteristics between Autonomous Mobile Robots in a Small I4.0 Manufacturing Facility

Troels B. Sørensen*, Rasmus L. Bruun*, Rene D. Marcker, and Preben E. Mogensen*
*Wireless Communication Networks Section, Department of Electronic Systems, Aalborg University, Denmark
Email: tbs@es.aau.dk, rlb@es.aau.dk, pm@es.aau.dk

***Abstract*—The use of millimeter wave communication for replacing wires in industrial environments has received much interest as part of the Industry 4.0 revolution. MM-wave communication may be used to have manufacturing entities communicate device to device in a decentralized private communication network, e.g. for letting autonomous mobile robots cooperate for improved efficiency and speed. Our objective in this paper is to understand how the device to device channel may be different from the characteristics reported in the literature on the infrastructure-based communication channel, as well as between cm- and near mm-wave. By transmitting and measuring a 5G synchronization signal burst, time-synchronized with the position of two moving robots, we characterize the large- and small-scale propagation characteristics as a function of the line of sight distance within a cluttered manufacturing space. Overall, we find only small differences between 3.8 and 26.4 GHz, however, with a clear indication that propagation at 26.4 GHz is more dominated by the geometric line of sight condition. For distances up to 35 m, path loss characteristics at the two frequencies are almost identical, close to free space propagation, and with shadowing decorrelation according to the (Gaussian) exponential decay model.**

***Index Terms*—Device to device, Industry 4.0, cm-wave, mm-wave, channel characteristics, Rician fading**

I. Introduction

Wireless technology is a key element in the Industry 4.0 (I4.0) revolution, enabling greater flexibility in production and manufacturing by replacing previously wired logic controllers and sensors/actuators deployed in connection with machines, tools and work pieces. The continuing 5G standardization efforts to meet stringent requirements for high reliability, low latency and high throughput have spurred the interest with companies to have private wireless communication networks [1]. For many use cases, the traditional infrastructure-based network is a good solution, i.e. enabling wireless communication by having one or more base stations deployed throughout the manufacturing environment. This case suits particularly well when there is a need for centralized control. But there are also use cases which are more eligible for distributed control, particularly cases where there is a need for collaboration between devices, such as collaborating manufacturing robots or autonomous mobile robots for moving goods around the factory. In these cases, direct device-to-device (D2D) communication caters for reduced latency and higher throughput, thereby enabling shared perception (vision), fast collaboration action/reaction and swarm behavior [1].

Many regulatory authorities have already allocated spectrum in the 5G cm-wave frequency range 1 (FR1) below 6 GHz, and are proceeding to allocate spectrum in the FR2 range above 24.25 GHz (referred here as mm-wave, as is commonly done in the context of 5G), which can be specifically suitable for communication between devices in proximity. Knowing the characteristics of the channel between devices is important in the design of D2D communication schemes, e.g. for distributed resource allocation as in our previous work in [2], [3]. Previous studies in connection with the WINNER II project [4], [5] indicated that there was no significant frequency dependence with respect to the fading statistics in the FR1 frequency range. The frequency independence was extended in [6] for 3GPP standardization to cover the 0.5–100 GHz band for indoor factory environments among others. Some recent studies in industrial environments have been published in [7] for FR1, [8] for FR2, and [9] for FR1 and FR2. In these papers, the focus was on both the large-scale, directional, and temporal dispersion characteristics for infrastructure-based communication, i.e. fixed base station to mobile device. Papers [8] and [9] argue for new scenarios to be included to [6] to properly capture the unique characteristics of industrial environments, e.g. the path loss characteristics which are claimed highly scenario dependent. Also, reference [10] studied propagation between FR1 and FR2, focusing on path loss and Rician fading statistics.

Different from all these previous studies, our main contribution in this paper is to investigate the D2D channel characteristics between mobile robots in an industrial environment. The questions we initially posed were whether this channel, with both ends of the link in the clutter, behave similarly to the infrastructure-based case, and whether characteristics are different between the two frequency bands. We focus, similar to [10], on the large-scale and small-scale (Rician) fading characteristics between the FR1 and FR2 frequency bands, but also analyse the correlation behavior in shadow fading and the behavior of fading statistics relative to the physical environment.

978-1-6654-7318-7/22/$31.00

Fig. 1. Situation from the Smart Production Lab, showing the MiR®200 carrying the transmitter setup.

II. Measurement Description

Our measurements have been conducted in the Smart Production Laboratory at Aalborg University, Denmark. The lab is used for research and educational purposes, and constitutes a small I4.0 based manufacturing facility, equipped with several tool stations, conveyor belts, moving robots, etc. Concerning the dimension and layout, it is generally similar to the machine shop in reference [11], and in between the range of indoor factory scenarios considered in [6]. Fig. 1 shows a situation from the lab where some of the tool stations can be seen distributed over the floor space. The lab is rectangular with an arterial passage through the center and with branched paths on both sides. It has a width of 14 m and a length of 42 m. The ceiling height is 6 m, but with several metallic structures filling the upper part, e.g. large ventilation ducts as seen in Fig. 1.

A. Measurement setup and procedure

Two MiR®200 Autonomous Mobile Robots (AMRs) have been used in the measurements, one carrying the measurement transmitter and the other the receiver. The MiR robots are equipped with Simultaneous Localization and Mapping (SLAM) capability which make them capable of autonomously navigating the environment based on a set route. The AMRs were pre-programmed with specific routes to cover most of the lab, and so that they take different paths. On average, they moved with a speed of 0.1 m/s. Each AMR was connected to a Raspberry Pi® unit via the *RESTful* application programming interface. Using this interface, the Pi units stored position data, relative to a local reference frame, at a rate of 10 Hz. The Pi's also acted as WiFi-connected Network Time Protocol (NTP) clients towards a local NTP server which synchronized timing on all position and measurement data to within 10 ms (99^{th} percentile). This setup allows the computation of the Euclidean distance, d, between the transmitter and receiver antennas to within an estimated ± 0.3 m (and often better), with inaccuracy mainly determined by the positioning accuracy of the AMRs. Fig. 2 shows an example of a drive path through the production lab, illustrating how the MiR robot perceives the environment clutter through its SLAM system.

Fig. 2. Example of SLAM output from one of the MiR®200 AMRs.

The measurement system is based around two main instruments from Rohde & Schwarz (R&S). At the transmitter side, we use an R&S®SMBV100B vector signal generator to generate a 5G NR synchronization signal in the FR1 and FR2 frequency bands, respectively. The synchronization signal block (SSB) contains primary/secondary synchronization (PS/SS) and physical broadcast channel (PBCH) signals [12]. It spans four orthogonal frequency division duplex (OFDM) symbols and 240 subcarriers as illustrated in Fig. 3. When performing the measurements we specifically used the SS signal (SSS) which occupies 3.81 MHz and 15.24 MHz (127 subcarriers) in FR1 and FR2, respectively. The transmitted signal was amplified and, for FR2, also upconverted, by an own developed module, to generate a conducted total output power of +17.9 dBm at the SS reference frequency (SSRef) of 3.792 GHz, and +13.1 dBm at SSRef of 26.42736 GHz. For the transmitter and the receiver, we used an omni-directional 3–40 GHz biconical antenna from A-info® (SZ-3004000/P), placed at a height of 1.6 m. The antenna has a maximum gain in the horizontal plane of 1.5 dB at the FR1 frequency and 5.0 dB at the FR2 frequency.

At the receiver side, we use an R&S®TSME6 radio scanner together with a TSME30DC down-converter for the 26–30 GHz range. To split the power from one receive antenna to separate frequency inputs on the TSME30DC we use a diplexer followed by a pre-amplifier for the FR2 frequency range, which leads to a combined noise figure for the receiver part around 6 dB in both FR1 and FR2 frequency ranges. Overall, the transmitter - receiver setup provides a maximum

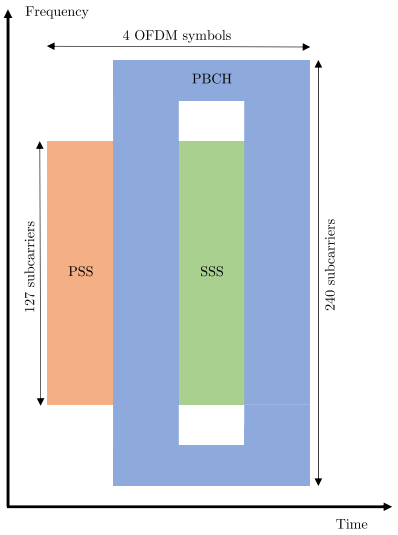

Fig. 3. Structure of the 5G synchronisation signal burst within the SSB.

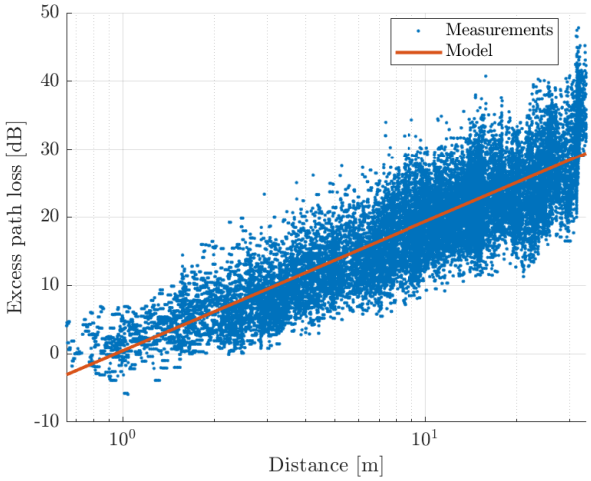

Fig. 4. Excess path loss at FR1 according to (1); blue dots are measurements, p_{rx}, and solid red line is according to the model in (3).

dynamic range of approximately 120 dB.

For the measurements in the lab, we first measured the D2D channel at FR1, and then in a separate measurement, at FR2. The measurements were prepared as described above, using the same equipment but different settings for the transmitter and receiver to generate the SSB signals. We obtained one measurement of the SSS resource element power, p_{rx}, i.e. the average power over the SSS bandwidth, nominally every 20 ms. To help average out the noise, two consecutive SSB signal bursts for FR1, and four for FR2, were averaged over the 5 ms duration of the SSB. With an average speed of 0.1 m/s, relatively the two robots could move at 0.2 m/s (worst case), but since their individual paths involve many turns and deceleration/accelerations this is considered an extreme case. Assuming the relative speed to be 0.1 m/s on average, the two robots move 0.025 wavelengths relative to one another per 20 ms at FR1 (wavelength of $\lambda = 81.0$ mm) and 0.180 wavelengths per 20 ms at FR2 (wavelength of $\lambda = 11.3$ mm).

III. Analysis and Results

The resulting measurand, p_{rx}, has been analyzed with respect to large-scale, i.e. average path loss and shadow fading, and small-scale fading. First, to derive the average path loss, we obtained a measure of the average power at a reference distance of $d_{ref} = 1$ m by averaging eight p_{rx} measurements distributed equally in angle circumferentially to the transmitter, rotating also the receiver antenna around the circumference, to average out variations in the H-plane patterns of the biconical antennas. The resulting (omni-directional) average, $\overline{p}_{rx\_ref}$, was used to define the *excess path loss* PL_{ref} in relation to the total path loss PL as a function of the direct LOS distance d; in decibel units:

$$PL_{ref}(d) = \overline{p}_{rx\_ref}(d_{ref}) - p_{rx}(d) \quad (1)$$

$$PL(d) = PL_{ref}(d) + 20\log_{10}\left(\frac{4\pi}{\lambda}\right) \quad (2)$$

Since the transmit power and antenna gains are included to both $\overline{p}_{rx\_ref}$ and p_{rx} they cancel out in (1); the only additional loss, assuming a constant omni-directional antenna gain and free space condition in measuring $\overline{p}_{rx\_ref}$, is therefore the second term in (2) which represents the coupling factor: at FR1 the coupling factor amounts to 43.8 dB and at FR2 to 60.9 dB.

Concentrating on the excess path loss, we enforce the log-distance model for the large-scale characterisation, cf. (3): in this model, the deterministic part is characterized by the path loss exponent γ, and the stochastic part by χ representing the aggregate of random large- and small-scale fading.

$$PL_{ref}(d) = PL_{offset} + 10\gamma\log_{10}(d/d_{ref}) + \chi \quad (3)$$

The model is shown in Fig. 4 and 5 overlaid on the respective measurements. In both figures, we have estimated the model parameters by least squares regression by including an offset parameter, PL_{offset}, in (3) to allow the least sum of squares and hence the best fit to the data. Although the offset is negative by -2.9 dB for FR2, the offset is only $+0.5$ dB for FR1, attesting to the theoretical formulation in (2) (at $d = d_{ref}$, the average PL equals the theoretical coupling factor, with zero offset). In general, it can be seen that the single slope model fits the data well up to distances of 35 m between the two robots. Note, we have included only measurements with maximum total path loss, as per (2), up to 100 dB, i.e. 20 dB below the dynamic range of the measurement setup.

A path loss exponent of 1.9 is observed at both frequencies, cf. Table I, thus suggesting near free space propagation characteristics. Slopes both below and above, but similar, have been reported in other studies for industrial environments, e.g. [11] with slopes of 1.9 and 1.6 in FR1, and [10] with slopes of 1.9–2.2 for LOS and 2.2–2.6 for NLOS conditions, with the lower values for FR1 and the higher ones for FR2. Reference [9] reported higher values under similar conditions, with 2.3 for LOS and 3.0 for NLOS, but also quoted studies that

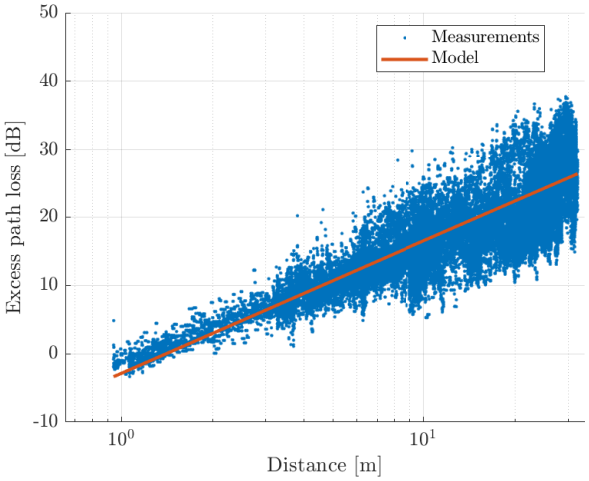

Fig. 5. Excess path loss at FR2 according to (1); blue dots are measurements, p_{rx}, and solid red line is according to the model in (3).

came to lower values. As demonstrated in [7], [10], values are dependent on the height of the transmitter and receiver. This explains part of the differences between the studies, and to our D2D case. The high number of samples collected with our approach attests to the validity of the estimated slopes: in this (near free space) condition, we should expect the same path loss slopes for FR1 and FR2, as only the offset is impacted by the operating frequency (cf. (2) and (3)).

A. Large-scale fading

For evaluation of the large-scale (shadow) fading, we first average the resource element power measurements, p_{rx}, over 40 wavelengths to remove the impact of small-scale fading, and then normalize the resulting values according to the deterministic part of the model in (3). The resulting residual (shadow fading) is approximately zero mean Gaussian distributed, with a standard deviation of 2.5 dB and 2.4 dB for FR1 and FR2, respectively, which is comparable to the values reported in [9], [10], but lower than the approximate 5–7 dB specified in [6]. Another interesting property related to shadow fading is the decorrelation distance, determined from the autocorrelation properties of the residual. The single decay large-scale fading autocorrelation model was suggested by Gudmundson in [13] for fixed base station to mobile device. The model was extended by Wang et al. in [14] to allow for mobility of both endpoints such that the autocorrelation function (ACF) is expressed as (note, we left out $ln(2)$ in the argument to define d_{cor} at the more common level of e^{-1})

$$R(d_T, d_R) = \exp\left(-\frac{|d_T| + |d_R|}{d_{cor}}\right) \tag{4}$$

where $|d_T|$ and $|d_R|$ are the distances traveled by the respective AMRs, and d_{cor} is the *decorrelation distance*, i.e. the distance at which $R(d_T, d_R) = e^{-1}$ (note that $|d_T| + |d_R|$ represents distance along the path and hence is different from d). Fig. 6 (FR1) and 7 (FR2) show the sample autocorrelation function

TABLE I
LARGE-SCALE PATH LOSS PARAMETERS - PATH LOSS SLOPE, SHADOWING STANDARD DEVIATION AND SHADOWING DECORRELATION DISTANCE.

	γ	σ_L	d_{cor}
FR1	1.9	2.5 dB	7.7 m
FR2	1.9	2.4 dB	5.2 m

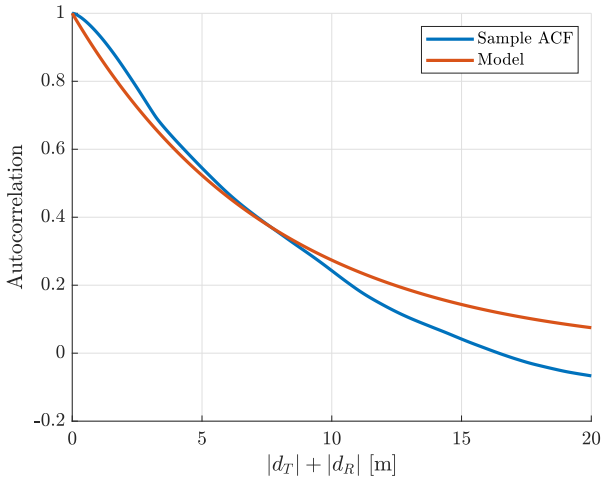

Fig. 6. FR1 sample autocorrelation function shown together with the exponential decay model.

together with the model in (4), assuming the decorrelation distance determined from the sample ACF. Notably, the decorrelation distance is the main difference between the two frequency ranges, with FR1 $d_{cor} = 7.7$ m and FR2 $d_{cor} = 5.2$ m. These values are lower than the 10 m suggested by 3GPP [6]. Table I summarizes the respective model parameters for the two frequency ranges.

B. Small-scale fading

Small-scale fading is what remains after normalising the measurand, p_{rx}, by its average over 40 wavelengths, i.e. removing large-scale effects caused by average path loss and shadowing. Due to the observed large-scale behavior and high probability of LOS between transmitter and receiver, we use Rician fading as a descriptive model. In Rician fading, the amplitude gain follows a Rician distribution with probability density function $f_X(x)$ given as [15]:

$$f_X(x) = \frac{s}{\sigma^2} \exp\left(-\frac{x^2 + s^2}{2\sigma^2}\right) I_0\left(\frac{xs}{\sigma^2}\right) \tag{5}$$

where I_0 is the modified zeroth order Bessel function of the first kind. The Rician distribution has two parameters, the non-centrality parameter s and the scale parameter σ. Alternatively, it can be specified in terms of the scale parameter $\Omega = s^2 + 2\sigma^2$, equivalent of the total power from all propagation paths, and the shape parameter, K, commonly referred as the K-factor, being similarly equivalent to the ratio between the power of the specular (LOS) component, s^2, and the power of the scattered and random multi-path components, $2\sigma^2$, thus

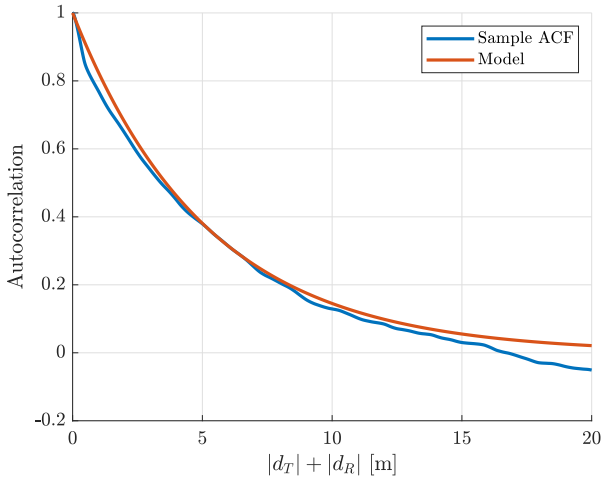

Fig. 7. FR2 sample autocorrelation function shown together with the exponential decay model.

$K \equiv s^2/2\sigma^2$. When no LOS component exists, i.e. $K = 0$, the amplitude distribution degenerates to the Rayleigh distribution.

From the measurements, we estimate the K-factor by maximum likelihood estimation of the Rician distribution parameters s and σ, and use the previous relation to calculate the K-factor; the estimation is based on 1000 samples of the small-scale fading envelope, equivalent of 25 and 180 wavelengths at FR1 and FR2, respectively, at a relative robot speed of 0.1 m/s and sampling period of 20 ms (12 wavelengths at FR1 and 90 at FR2 worst case at a relative speed of 0.2 m/s). Estimations have been checked against the moment-based method in [15], leading to results that deviate in absolute value by maximum 0.43 (in mean, 0.08, and standard deviation 0.07) and therefore in practice identical results. In both cases, the estimation is rather insensitive to the number of samples, for instance, using a few hundred samples leads to almost identical results.

Due to the difference in transmit bandwidth for the SS-signal in FR1 and FR2, the measurand will be subjected to different amounts of frequency averaging. Frequency averaging will decrease the K-factor corresponding to the number of frequency coherence bandwidths inside the measurement bandwidth. In case of linear averaging of the complex envelope, the K-factor directly increases by the averaging factor (variance reduction of independent and identically distributed Gaussian variables). In our case, with power (envelope) averaging, that relation is only approximately true because, contrary to the former case, the resulting distribution is not Rician. Still, one can approximate with a Rician distribution and estimate a K-factor, but with the effect that it will increase slightly more than the number of coherence bandwidths from an average perspective. Typical coherence bandwidth for FR1 and FR2 in an indoor factory environment is in the range 3-4 MHz [9], which corresponds to the FR1 measurement bandwidth. Since the FR2 measurement bandwidth is four times larger, suggesting four times the K-factor with linear averaging, due to the non-linear averaging we scale the estimated FR2 K-factors by a factor of $1/4.5$ to make the comparison to FR1 (the scaling effect is closer to $1/5$ for K values below 15 and closer to $1/4$ for values above, including also effects from the finite number of samples and number of samples per wavelength).

Fig. 8 and Fig. 9 show the resulting K-factors. At the top of the plots, we show the estimate as a function of the sample number in comparison to the LOS distance between the two robots. The geometric LOS condition is shown overlaid, based on analyzing the SLAM output in Fig. 2 in relation to the positions of the robots at a given sample/time; green color is used to indicate the LOS condition. Particularly, in Fig. 9 there is a clear (visual) correlation between geometric LOS condition, (low) distance and (high) K-factor, and from Fig. 8 less so, suggesting that propagation at FR2 is more dominated by geometric LOS. Being statistics, it can happen of course that large distance is associated with high K-factor (with no geometric LOS), as can be seen in Fig. 9 between sample no. 130,000 and 140,000, or short distance with high K-factor, as seen close to sample no. 54000, but there is a clear trend that propagation is different between the two bands in this respect. Looking at the lower part of the figures, we see higher K-factors at FR2 and a pronounced effect of having higher values at shorter distances. The distance effect at FR2 is however visible only at very short distances, and essentially absent at FR1. This is generally in good agreement with the observed correlation between K-factor and distance for FR1 and FR2, as well as the increasing standard deviation in Fig. 5 for FR2. The exact paths and relative positions of the two robots at a given time were different between the two measurements, and a smaller number of measurement samples were collected at FR1 due to a temporary interruption. This led to more LOS/NLOS conditions at FR2, but despite and in line with intuition, we see that in both cases, LOS is more likely to happen with shorter distances between the robots (note that the K-factor plots at the bottom cover distances up to 35 m only, which is where we have a reasonable number of estimates per distance interval). Contrary to the assumptions in [6], we see frequency dependency with higher K-factors in FR2. This is consistent with the findings in Guan et al. [10] where they similarly observe a slight increase of the K-factor at FR2 compared to FR1, and some distance dependency at FR2 but not at FR1. Both Guan's and our study observe overall similar values of K-factor compared to the average values of 7 dB (5 in linear) in [6] and 5.5 dB (3.5 in linear) in [11]. The K-factor correction explained earlier has minimal impact on the observed behavior, but introduces some uncertainty to the absolute level of the K-factor at 26.4 GHz. Additionally, the radiation pattern of the biconical antennas has some differences between FR1 and FR2: both antennas are approximately omni-directional in the H-plane, however, the E-plane is considerably narrower at FR2 (half power beam width of around 36 versus 120 degrees), acting to reduce multipath in the elevation plane and thus principally increasing the K-factor. Multipath in the elevation plane is plausible,

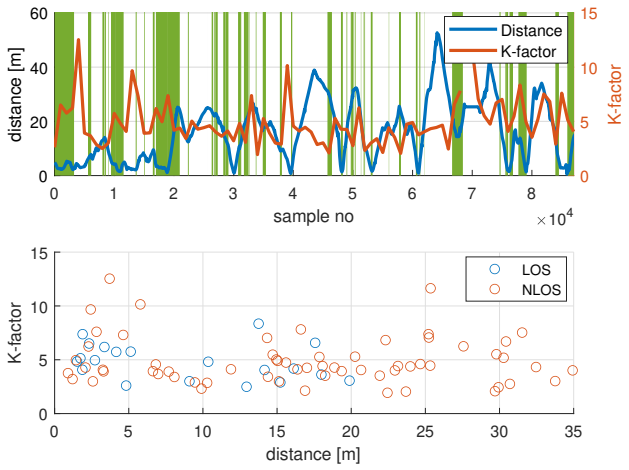

Fig. 8. K-factor in FR1 in comparison to direct LOS distance: (top) distance and K-factor versus sample no. - green indicates geometric LOS condition; (bottom) K-factor versus direct LOS distance.

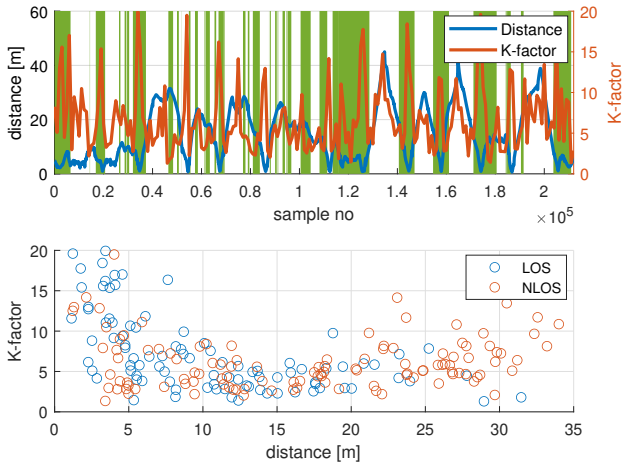

Fig. 9. K-factor in FR2 in comparison to direct LOS distance: (top) distance and K-factor versus sample no. - green indicates geometric LOS condition; (bottom) K-factor versus direct LOS distance.

but it needs to take a longer path compared to multipath in the immediate surroundings of the transmitter-receiver couple. For both impacts, we have accounted for the main effects and therefore assume results to be representative.

IV. Conclusion

In this paper, we presented a comparison of channel characteristics between cm- and near mm-wave frequencies for the device-to-device (D2D) channel in a small manufacturing facility. The D2D channel is of interest for the design of communication schemes in the context of Industry 4.0, e.g. for enabling shared perception between collaborating autonomous mobile robots.

Based on measurements of a 5G NR FR1 and FR2 synchronization signal burst, we analysed the large-scale, i.e. average path loss and shadow fading, and small-scale fading characteristics as a function of distance between two moving autonomous mobile robots. Overall, we noticed only small differences between the two frequency bands. For the large-scale characteristics, the log-distance model with path loss slope of 1.9 made a good representation to the measurements for distances up to 35 m, with shadow fading being approximately Gaussian distributed, zero mean, and of standard deviation close to 2.5 dB, irrespective of the frequency band. The decorrelation of the shadow fading follows the single exponential decay model as a function of sum of distance moved by transmitter and receiver jointly, with decorrelation distances in the range 5–8 m. In the small-scale fading characteristics, we see Rician K-factors in the same range for the two frequencies, but with a clear indication that propagation at mm-wave has a stronger correlation to geometrical LOS, and with K-factors clearly increasing at short distances. Our findings are generally comparable to reported characteristics for the infrastructure-based communication channel in similar environments.

References

[1] I. Rodriguez *et al.*, "5g swarm production: Advanced industrial manufacturing concepts enabled by wireless automation," *IEEE Communications Magazine*, vol. 59, no. 1, pp. 48–54, Jan. 2021.

[2] S. Morejon *et al.*, "Cooperative resource allocation for proximity communication in robotic swarms in an indoor factory," in *2021 IEEE Wireless Communications and Networking Conference (WCNC2021)*, Nanjing, China, Mar. 2021.

[3] ——, "Decentralized cooperative resource allocation with reliability at four nines," in *2021 IEEE Global Communications Conference (GLOBECOM)*, Madrid, Spain, Dec. 2021.

[4] D. Baum *et al.*, "An interim channel model for beyond-3g systems: extending the 3GPP spatial channel model (scm)," in *2005 IEEE 61st Vehicular Technology Conference*, vol. 5, 2005, pp. 3132–3136 Vol. 5.

[5] P. Kyösti *et al.*, "WINNER II channel models," *IST-4-027756 WINNER II D1.1.2 V1.2*, 02 2008.

[6] 3rd Generation Partnership Project (3GPP), "Study on channel model for frequencies from 0.5 to 100 GHz," in *3GPP TR 38.901 V16.1.0*, Dec. 2019.

[7] M. Razzaghpour *et al.*, "Short-range UWB wireless channel measurement in industrial environments," in *2019 IEEE International Conference on Wireless and Mobile Computing, Networking and Communications (WiMob)*, Barcelona, Spain, Oct. 2019.

[8] M. Schmieder *et al.*, "Directional wideband channel measurements at 28 GHz in an industrial environment," in *2019 IEEE IEEE Global Communications Conference (GLOBECOM)*, Waikoloa, USA, Dec. 2019.

[9] ——, "Measurement and characterization of an indoor industrial environment at 3.7 and 28 GHz," in *2020 IEEE 14th European Conference on Antennas and Propagation (EuCAP)*, Copenhagen, Denmark, Mar. 2020.

[10] Y. Guan *et al.*, "A comparative study for indoor factory environments at 4.9 and 28 GHz," in *2020 14th European Conference on Antennas and Propagation (EuCAP)*, 2020.

[11] R. Candell *et al.*, "Industrial wireless systems radio propagation measurements," *NIST Technical Note 1951*, pp. 1–125, 2017.

[12] 3GPP, "TS 38.215 V16.4.0 physical layer measurements," Dec. 2020.

[13] M. Gudmundson, "Correlation model for shadow fading in mobile radio systems," *Electronics Letters*, vol. 27, no. 23, p. 2145, 1991.

[14] Zhenyu Wang, E. Tameh, and A. Nix, "Joint shadowing process in urban peer-to-peer radio channels," *IEEE Transactions on Vehicular Technology*, vol. 57, no. 1, pp. 52–64, Jan. 2008. [Online]. Available: http://ieeexplore.ieee.org/document/4357088/

[15] F. V. d. Wijk, A. Kegel, and R. Prasad, "Assessment of a picocellular system using propagation measurements at 1.9 GHz for indoor wireless communications," *IEEE Transactions on Vehicular Technology*, vol. 44, no. 1, pp. 155–162, Feb. 1995. [Online]. Available: http://https://ieeexplore.ieee.org/document/350281